Effects of fluctuating thermal sources on a shell-and-tube latent thermal energy storage during charging process

H I G H L I G H T S

- Melting process of LTES under fluctuating thermal sources analysed
- Fluctuating period and amplitude of fluctuating heat sources investigated
- Large-period fluctuating heat sources significantly accelerate the melting process
- Melting rate increases but energy storage capacity decreases with amplitude rising
- Larger *Ste* reduces gap of melting rate between small and large period heat sources

Abstract: The fluctuating and intermittent nature of industrial heat sources is a crucial technical barrier limiting the implementation of heat recovery energy systems. Latent Thermal Energy Storage (LTES) has the potential to overcome these issues by maintaining a Waste Heat Recovery (WHR) system within designed operation conditions to achieve effective and efficient operation. However, the dynamic heat transfer characteristics of LTES under fluctuating heat sources need to be studied further to better understand the effects of thermal fluctuation. In this work, the charging performance of a shell-and-tube LTES under fluctuating and steady heat source has been investigated and analysed. The effects of period and amplitude for the fluctuating heat source, as well as the Stefan number, are investigated in detail. Results indicate that large-period fluctuating heat sources can considerably reduce the total melting time but also reduce the energy storage capacity, whilst small-period fluctuating heat sources have almost no effect on the melting process of LTES. For the effects of fluctuating amplitude, both the total melting

time and energy storage capacity decline at a decreasing rate with an increase of fluctuating amplitude. These results can bridge the knowledge gap needed for future designs of shell-and-tube LTES for fluctuating heat sources used with heat recovery applications.

Keywords: Thermal energy storage, Phase change material, Waste heat recovery, Fluctuating thermal source, Shell-and-tube heat exchanger

Nomenclature	
A	Fluctuating amplitude of heat source (K)
$c_{p,f}$	Specific capacity of heat transfer fluid (J/kg K)
$c_{p,p}$	Specific capacity of phase change material (J/kg K)
f	Liquid volume fraction
H	Total enthalpy of phase change material (J/kg)
h	Sensible heat of PCM (J/kg)
L	The latent heat of PCM (J/kg)
p	Pressure (Pa)
P	Fluctuating period of heat source (s)
ref	Reference state
r_i	Radium of inner tube (m)
r_o	Radium of outer tube (m)
T_{av}	Average temperature of heat source (K)
T_m	Melting temperature of PCM (K)
Greek letters	
α	Thermal expansion coefficient (K^{-1})
λ	Thermal conductivity (W/m K)
μ	Dynamic viscosity (Pa s)
ρ	Density (kg/m^3)
ε	Constant number

1. Introduction

Organic Rankine Cycle has been widely recognised as a technology with the greatest potential to recover industrial waste heat, due to its high efficiency, high reliability and low cost [1, 2]. However, most of the available industrial heat sources possess a fluctuating and intermittent nature, resulting in a crucial technical barrier limiting the implementation of ORC-based WHR systems [3]. The instability of industrial heat sources leads to ORC systems operating under off-design conditions with low efficiency [4]. Latent Thermal Energy Storage (LTES)using Phase Change Materials (PCMs) is a potential solution to buffer the fluctuation of industrial heat sources [5, 6]. PCM-based thermal energy storage systems absorb heat from the waste heat source and then release the stored heat to the WHR systems. Such systems can overcome the fluctuation of heat sources and maintain ORC systems within their design conditions.

A wide range of LTES using PCMs have been applied and studied in solar power plants and solar heating systems [7, 8]. For example, Li *et al.* [9] investigated the dynamic performance of a solar ORC system integrated with LTES to overcome solar disturbance. In the study, LTES is considered as a homogeneous heat capacity system without taking account of the internal heat transfer process. Results showed that fluctuating period and amplitude of solar radiation affected the selection of optimal LTES volume and then influenced the ORC performance. As well as reducing the instability of solar radiation, LTES has also been applied to improve the matching performance of end-user demands in small-scale solar ORC systems and domestic-scale solar heating system. A representative work reported by Freeman *et al.* [10] from Imperial College London discussed the different thermal energy storage solutions for a domestic-scale solar CHP system to meet the heat and electricity demand during the night. The authors focused

on the energy storage performance of LTES without considering its heat transfer performance under dynamic inlet parameters. The results demonstrated the importance of LTES design on system performance. However, due to the variation of solar radiation over significant timescales and demand for energy storage, most of the studies undertaken to date have generally neglected the effects of fluctuation of solar radiation on the heat transfer performance of LTES and paid more attention to the system operating performance and the design/optimisation of LTES.

In the application for industrial waste heat recovery, LTES also plays an important role to bridge the gap between the heat sources and heat recover energy systems. Fabio *et al.* [11] proposed a PCM-coupled steam generator for dynamic industrial waste heat recovery. In this study, the PCM was simplified as big heat capacity and the results indicated that the PCM-based system could significantly reduce the thermal power fluctuation of the heat source and enlarge the high-efficiency working zone. Yu *et al.* [12] designed an ORC system using the concept of double shell-and-tube LTES. This study considered the effects of PCM thermophysical properties and LTES volume on the performance of the proposed ORC system to recover fluctuating thermal energy. The results showed the superiority of a PCM-based combination system for fluctuating heat source without considering the detailed heat transfer process within the LTES. Xu *et al.* [13] concluded a forward-looking perspective demonstrating time-dependent heat recovery technologies integrating with thermal energy storage can address the time matching, spatial matching and energy grade matching between the energy source and demand, which is promising for use as a next-generation heat recovery technology.

Since the thermal behaviours of PCM have a significant influence on the charging-discharging process of LTES, reported numerical and experimental researches focused on the heat transfer characteristics of

the LTES systems under steady boundary conditions. Some studies investigated the effects of geometrical and thermophysical parameters and thermal boundary conditions on the melting process. Guo *et al.* [14] performed a numerical study to assess the effects of heat exchanger geometry and thermal boundary conditions on the energy storage performance of a vertical shell-and-tube LTES. Wang *et al.* [15] studied the effects of the temperature difference between the Heat Transfer Fluid (HTF) and the melting point of PCM, as well as the inlet mass flow rate, on the charging performance of a horizontal shell-and-tube LTES. Tao *et al.* [16] evaluated the effects of the PCM thermophysical properties on the charging performance of a high-temperature LTES unit. Other studies have concentrated on the heat transfer enhancement and heat exchanger design of LTES systems. Francis *et al.* [17] compared the melting process of three LTES systems with circular and longitude fins and without fins. Wang *et al.* [18] carried out a numerical study to analyse the melting process of shell-and-tube LTES under different geometrical parameters of fins, including fin length, fin ratio and fin angle. Heat pipes [19], nanoscale additives [20], porous media [21] and cascaded PCM [22] were also used to enhance the heat transfer performance of shell-and-tube LTES systems. The design of LTES heat exchangers has also attracted much attention in recent years. The design of LTES heat exchangers has also received much attention, as reported in recent studies. For example, Fang *et al.* [23] developed an analytical method to design the required heat transfer length and predict the energy storage ratio based on the effectiveness-NTU theory for any tube-in-tank LTES systems. Deng *et al.* [24] performed a numerical study to find out the optimal layouts of fins for a shell-and-tube latent LTES.

However, the majority of research on shell-and-tube LTES systems is based on steady thermal boundary conditions. When an unsteady heat source was considered, the detailed heat transfer process of PCM,

under fluctuating thermal boundaries, was not significantly addressed, investigated and examined in the previously reported studies. The majority of related studies conducted calculations by thermodynamic analysis or considering the PCM as large heat capacity. However, the fluctuation in inlet temperature or mass flowrate shown in **Fig. 1** should be considered in the design stage of LTES systems for industrial waste heat recovery. Because the characteristics of industrial heat sources, including the period and amplitude, are quite different from that of solar radiation, leading to different heat transfer and energy storage performance between the LTES systems designed based on steady and unsteady inlet parameters. Some researchers have noticed this challenge. In pioneering work, Tao *et al.* [25] numerically studied the charging performance of a shell-and-tube LTES under unsteady inlet temperature and mass flow rate with a linear variation. The results indicated that the larger initial inlet temperature and mass flow rate could substantially reduce the melting time of the paraffin LTES. Elbahjaoui *et al.* [26] evaluated the effects of laminar fluid flow with pulsed inlet pressure on the melting process of a shell-and-tube LTES unit. The numerical results showed that the inlet pressure of the laminar flow with low pulsating frequency and high pulsating amplitude could reduce the total melting time. Xu *et al.* [27] optimised the thermal performance of a cascaded shell-and-tube LTES system with a quadratic-variation inlet temperature of HTF from the perspective of exergy, entropy and entransy analysis. The optimised results showed that the optimal thermal performance of steady case was better than that of the fluctuating case. To increase the energy storage density and reduce the final average temperature of a solar LTES tank, Huo *et al.* [28] investigated the effects of the time-dependent intermittent heat flux on the energy storage performance. The proposed transient heat flux has the characteristic of square wave and its period and amplification were numerically evaluated. The results proved that the time-dependent heat flux could

reduce the final average temperature but increase the total melting time compared to the constant heat flux.

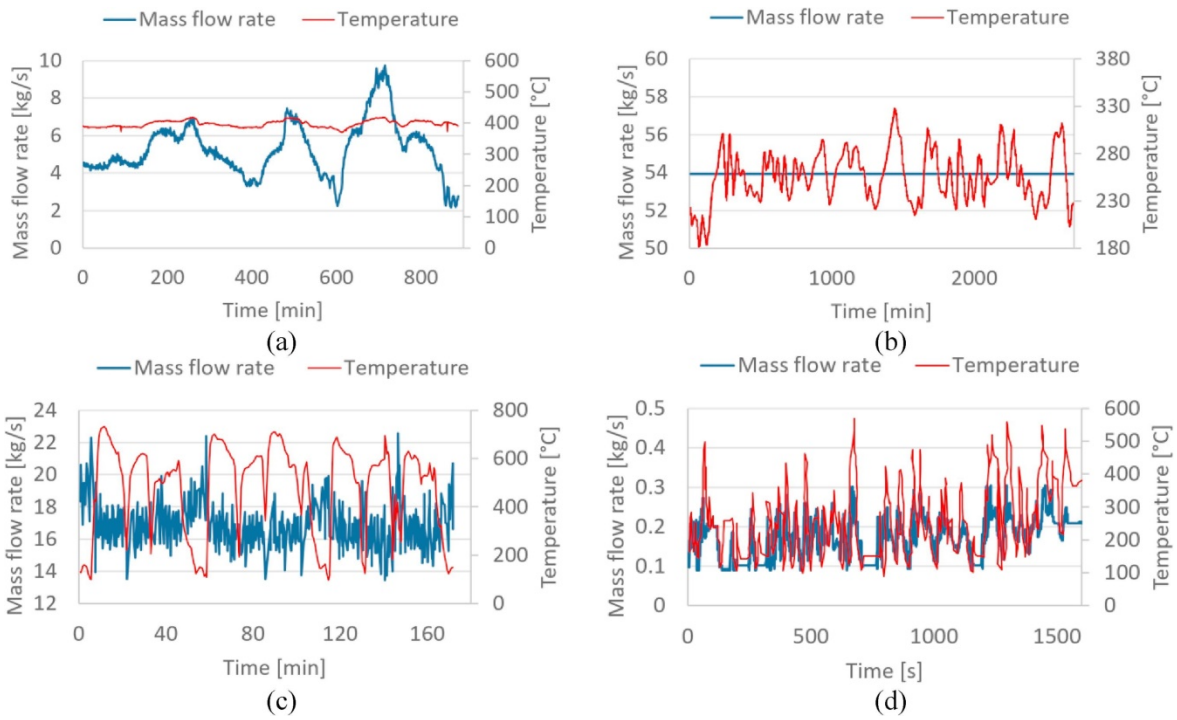

Fig. 1. Fluctuating characteristics of different waste heat source: (a) Steel billet reheating furnace; (b) Clinker cooling; (c) Electric arc furnace; (d) Internal combustion engine exhaust [29].

Based on the above literature study, it can be ascertained that the heat transfer process of a shell-and-tube LTES under sinusoidal inlet temperature has not been previously considered. Furthermore, the effects of different amplitudes, especially the periods to simulate different real industrial heat source shown in **Fig. 1** for sinusoidal heat sources should be determined. Therefore, in this study, the heat transfer process and energy storage performance of a shell-and-tube LTES heated by sinusoidal inlet temperature are investigated. In detail, the effects of different period and amplitude, as well as the Stefan number are analysed based on CFD simulations. The completion of this work contributes to our understanding of the heat transfer process of shell-and-tube LTES under fluctuating thermal boundaries,

as well as the design and optimisation of LTES units integrating with ORC-based WHR systems for industrial waste heat recovery.

2. Description of the simulation model

2.1 Physical model

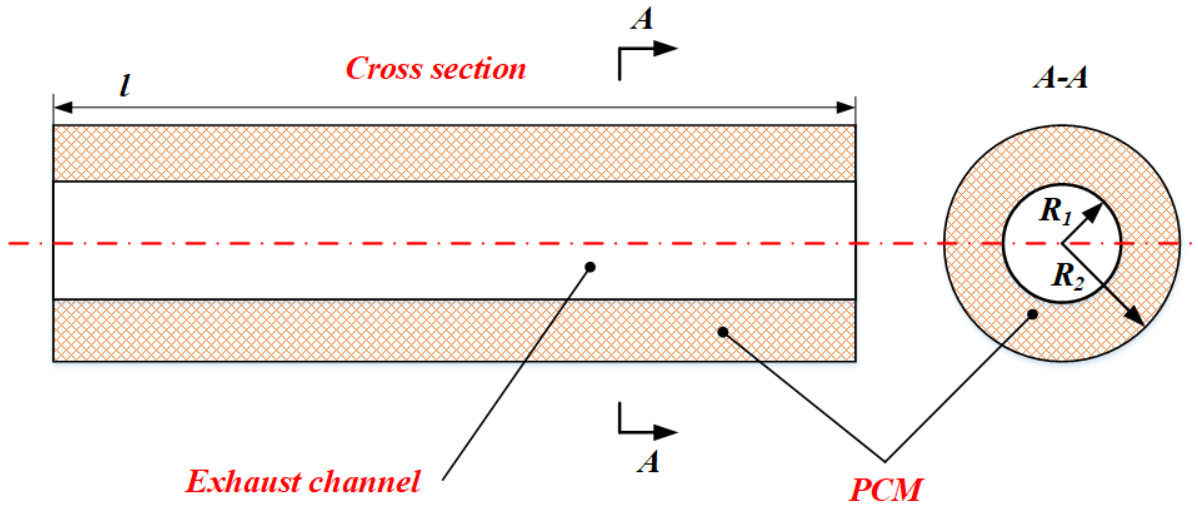

(a) (b)

Fig. 2. Sketch of the shell-and-tube latent thermal energy storage evaporator

(a) Front view in section, (b) Cross-sectional view

The heat exchanger, as illustrated in Fig. 2, is a typical cylindrical shell-and-tube LTES heat exchanger. The PCM is placed in the shell side while HTF flows through the tube side. The layout can maximise the heat transfer area of exhaust gas and PCM, as well as tolerate high-pressure fluid. The length of the LTES heat exchanger is 1000 mm, and the radius for the inner tube and outer shell are 12.5 mm and 25 mm respectively. Along the flow direction of HTF, each cross-section of PCM is heated by the fluctuating heat source and they undergo a similar heat transfer process. Therefore, a two-dimensional cross-section at the inlet of LTES has been selected as the physical model. Before establishing the

mathematical model, the following assumptions are adopted to simplify the physical model and later computation.

(1) The thermophysical properties of PCM are independent of temperature.

(2) The flow in the liquid PCM is assumed to be Newtonian laminar and incompressible.

(3) The thermal resistance of the inner wall is neglected while the outer wall of the LTES is adiabatic.

The thermophysical properties of the selected PCM are listed in **Table 1**.

Table 1 Thermophysical properties of the selected PCM

Parameters	PCM ($LiNO_3$-$NaNO_3$-KCl) [30]
ρ (kg/s)	2297
λ (W/m K)	0.88
c_p (J/kg K)	1330
μ (Pa s)	0.003
T_m (K)	433
ΔH (kJ/kg)	266
α (K^{-1})	0.0004

2.2 Governing equations

In this section, a two-dimensional transient heat transfer model for the cross-section of LTES based on the enthalpy method is presented to simulate the moving boundary problem within the PCM. The continuity equation for PCM is written as follows:

$$\frac{\partial \rho}{\partial t}+\frac{\partial(\rho u)}{\partial x}+\frac{\partial(\rho v)}{\partial y}=0 \tag{1}$$

In the enthalpy method, the energy equations for liquid state and solid state have the same form. The solid-liquid interface is indicated as a mushy zone to separate two phases. The energy equation for PCM is described as follows:

$$\frac{\partial \rho H}{\partial t}+\frac{\partial(\rho u H)}{\partial x}+\frac{\partial(\rho v H)}{\partial y}=\frac{\partial}{\partial x}\left(k\frac{\partial T}{\partial x}\right)+\frac{\partial}{\partial y}\left(k\frac{\partial T}{\partial y}\right) \tag{2}$$

Where H represents the total enthalpy of sensible enthalpy and latent enthalpy, which can be calculated by equation (3) and (4). h_{ref} denotes the sensible enthalpy at the reference temperature T_{ref}.

$$H=h+f\cdot L \tag{3}$$

$$h=h_{ref}+\int_{T_{ref}}^{T} c_p dT \tag{4}$$

Where f refers to the liquid volume fraction calculated by equation (5). It should be pointed out that the liquid volume fraction lies between 0~1 in the mushy zone.

$$f=\begin{cases} 0 & T<T_{solidus} \\ \dfrac{T-T_{solidus}}{T_{liquidus}-T_{solidus}} & T_{solidus}\le T\le T_{liquidus} \\ f=1 & T>T_{liquidus} \end{cases} \tag{5}$$

Substituting equation (3)-(5) into equation (2), the energy equation can be further written as:

$$\frac{\partial \rho h}{\partial t}+\nabla\cdot(\rho v h)=\nabla\cdot(k\nabla T)-\frac{\partial \rho f L}{\partial t}-\nabla\cdot(\rho v f L) \tag{6}$$

The natural convection makes a significant improvement in accelerating the melting process of LTES [31]. Due to the small variation in density, the natural convection is taken into consideration via the

Boussinesq approximation [32]:

$$(\rho-\rho_0)g=-\rho_0\beta(T-T_0) \tag{7}$$

Then the momentum equation considering natural convection for PCM has a form as follows:

$$\frac{\partial(\rho u)}{\partial t}+\frac{\partial(\rho uu)}{\partial x}+\frac{\partial(\rho uv)}{\partial x}=-\frac{\partial p}{\partial x}+\frac{\partial}{\partial x}\left(\mu\frac{\partial u}{\partial x}\right)+\frac{\partial}{\partial y}\left(\mu\frac{\partial u}{\partial y}\right)+A_{mush}u \tag{8}$$

$$\frac{\partial(\rho v)}{\partial t}+\frac{\partial(\rho uv)}{\partial x}+\frac{\partial(\rho vv)}{\partial x}=-\frac{\partial p}{\partial y}+\frac{\partial}{\partial x}\left(\mu\frac{\partial v}{\partial x}\right)+\frac{\partial}{\partial y}\left(\mu\frac{\partial v}{\partial y}\right)+A_{mush}v+\rho g\alpha(T-T_m) \tag{9}$$

In equation (9), the parameter A_{mush} is a constant to describe how quickly the velocity is decreased to zero when the PCM solidifies, which is calculated by [33]:

$$A_{mush}=-C\frac{(1-f)^2}{f^3+\varepsilon} \tag{10}$$

Where the constant ε is a very small number to prevent the division by zero.

2.3 Model of fluctuating heat source

As depicted in **Fig. 1**, the temperature of different heat sources can fluctuate over different periods varying between seconds, minutes and hours, as well as at different amplitudes. The fluctuating period and amplitude are important indicators to represent the characteristics of different fluctuating heat sources. To demonstrate how fluctuating heat sources affect the heat transfer process of the latent thermal energy storage, the effects of fluctuating periods and amplitudes for fluctuating heat sources need to be investigated. In this study, the inlet temperature of the fluctuating heat source is assumed as a sinusoidal function in the following equation:

$$T_{HTF}=a\cdot\sin(\pi t/b)+573 \tag{11}$$

When the effects of different periods and amplitudes are studied, the values of coefficients in formula (11) are listed in **Table 2** and **Table 3**, respectively. It should be pointed out that the average temperature of different fluctuating heat sources is fixed at 573 K for a one-hour period.

Table 2 Coefficient values of inlet temperature with different periods.

Cases	**a**	**b**
P=1 min	100	30
P=2 min	100	60
P=6 min	100	180
P=20 min	100	600
P=30 min	100	900
P=60 min	100	1800

Table 3 Coefficient values of inlet temperature with different amplitudes.

Cases	**a**	**b**
A=50 K	50	1800
A=75 K	75	1800
A=100 K	100	1800
A=125 K	125	1800
A=150 K	150	1800

2.4 Initial and boundary conditions

The initial conditions for PCM:

$$T_{PCM}\left(x,y\right)=T_m-10 \tag{12}$$

The boundary condition for HTF is:

$$T_{HTF,in}=T_{HTF} \tag{13}$$

The boundary condition for the outer wall is:

$$\frac{\partial T_{PCM}}{\partial r}\left(r=r_2\right)=0 \tag{14}$$

The boundary condition for the inner wall is:

$$h_{HTF}\left(T_{HTF}-T_{PCM}\right)=-k\frac{\partial T_{PCM}}{\partial r}\left(r=r_1\right) \tag{15}$$

3. Independency study and model validation

The computation is conducted using the software Ansys/Fluent 14.5. Before the simulation, the verification of grid size and time step are conducted. The computational domain is a two-dimensional annulus. The grid is created in three different sizes of 0.5 mm, 0.8 mm and 1 mm, corresponding to the grid number of 6006, 2384 and 1580. Meanwhile, four different time steps at 0.5 s, 1 s, 2 s and 5 s are also studied to demonstrate that the selected time step does not affect the computational results. **Fig. 3** shows the results of the verification of the time step and grid size. As a result of the verification results, the grid size of 0.8 mm (grid number of 2384) and a time step of 2 s are selected in the simulation model.

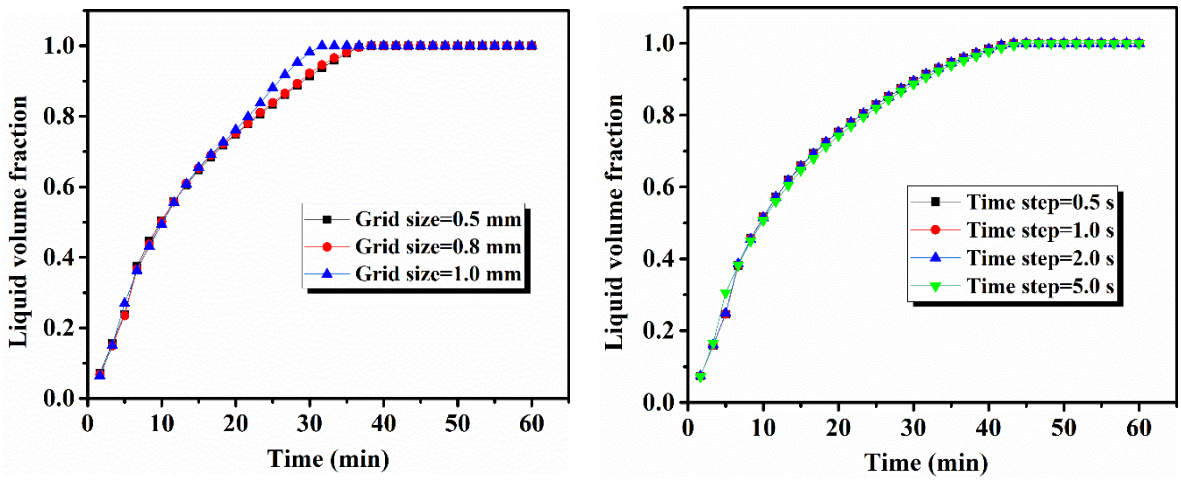

Fig. 3. Validation of the computational time step and grid size: (a) grid size; (b) time step.

A comparison between the present simulation and experimental results from reference [34] has been conducted to validate the numerical model. The comparative results are illustrated in **Fig. 4**. The reported temperature in the present simulation fits well with the experimental data in reference [34]. The error analysis indicated the maximum error between the present simulation results and experimental data in reference [34] is 4.67 %, which demonstrates the reliability and correction of the adopted numerical model.

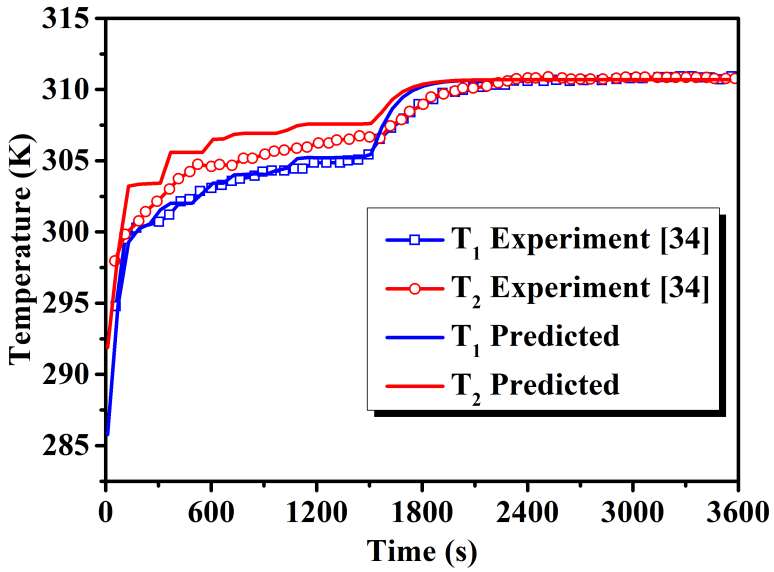

Fig. 4. The comparison between the present simulation and experimental results from reference

[34].

4. Results and discussion

4.1 Effects of fluctuating period

Fig. 5 shows the timewise liquid volume fraction of PCM heated by heat sources with different time periods. Because the fluctuating heat source is modelled as a sinusoidal function in the study, it is known that the temperature of the fluctuating heat source in the first-half period is higher than that of the second-half period, which indicated the PCM could absorb more heat from the fluctuating heat source during the first-half period than that of the second-half period. This explains why the liquid volume fraction increases at a faster rate in the first-half period and then increases at a much slower rate in the second-half period under fluctuating thermal source conditions, i.e., the evolution of liquid volume fraction presents a wavelike rise trend as shown in **Fig. 5**. Taking the case of P=20 min as an example, it can be found that the liquid volume fraction shows different increasing rates during the first and second half period across a whole period. In detail, the liquid volume fraction of P=20 increases quickly in the time-lag of 0~10 min, but it increases at a much lower rate in the time-lag of 10~20 min. The evolution trend of liquid volume fraction is similar to that of time-lag of 20~40 min. It can be shown that the wavelike rise trend is more significant for fluctuating heat sources with a larger period (P=20 min, 30 min, 60 min) rather than cases with a smaller period (P=1 min, 2 min, 6 min). The reason is that the difference in the heat transferred from HTF to PCM between the first and second half period is small for small-period fluctuating heat sources, while the difference is large for large-period cases during a whole period.

Compared to the constant heat source, it can also be shown that the fluctuating heat sources with a smaller period (P=1 min, 2 min, 6 min) have little effect on the evolution of liquid volume fraction, while the large-period (P=20 min, 30 min, 60 min) fluctuating heat sources can accelerate the melting process, especially in the early stage (t<20 min). In more detail, the liquid volume fraction under small-period fluctuating heat sources have a minor enhancement of liquid volume fraction in the early stage, but the improvement effects keep decreasing and finally, they only shorten the complete melting time of PCM to a very small extent. For large-period fluctuating heat sources, although the enhancement effects decrease after the early stage, they still reduce the total melting time to some extent according to the scale of the fluctuating period.

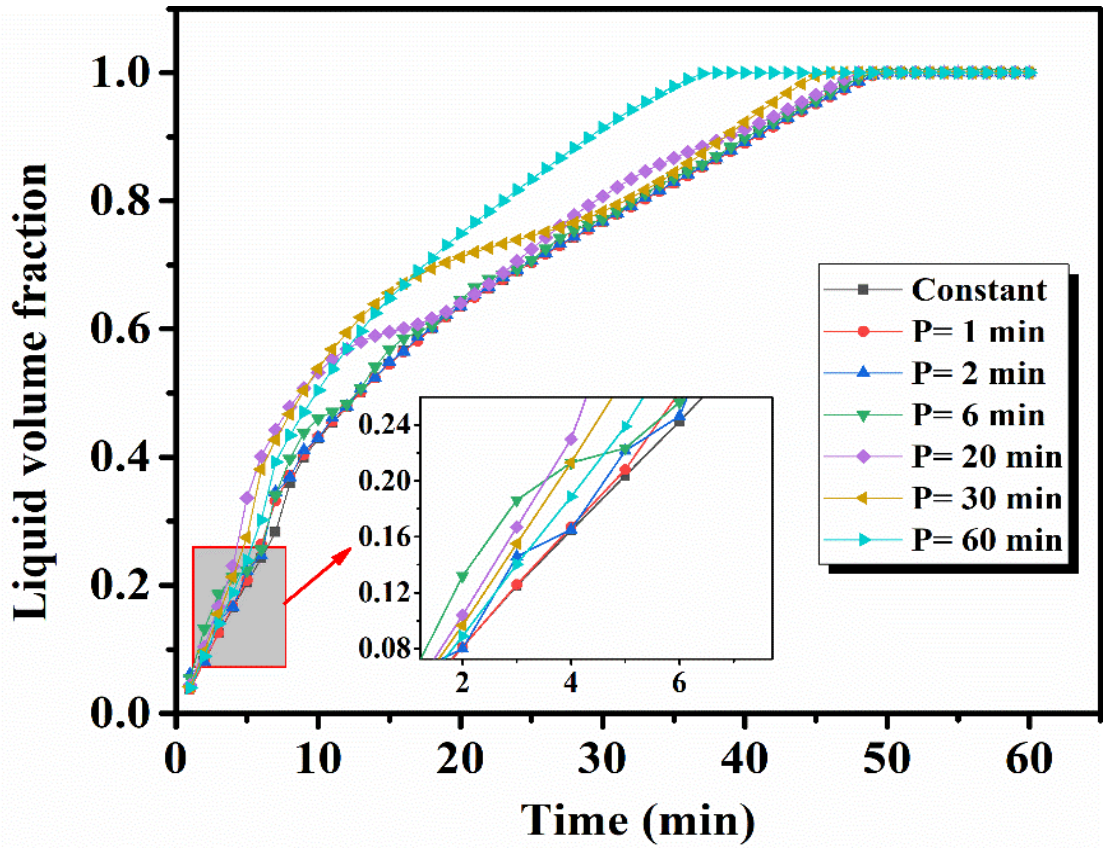

Fig. 5. The evolution of liquid volume fraction with melting time under different heat sources.

The total melting time for different heat sources is presented in **Fig. 6**. The values for small-period (P=1

min, 2 min, 6 min) fluctuating heat sources are 49.8 min, 49.7 min and 49.3 min, respectively, which are almost the same as the constant heat source (49.7 min). However, the total melting time decreases distinctly with the increase of the period for large-period (P=20 min, 30 min, 60 min) fluctuating heat sources, especially the total melting time (37.3 min) for the period of P=60 min is approximately 25% less than that of the constant heat source.

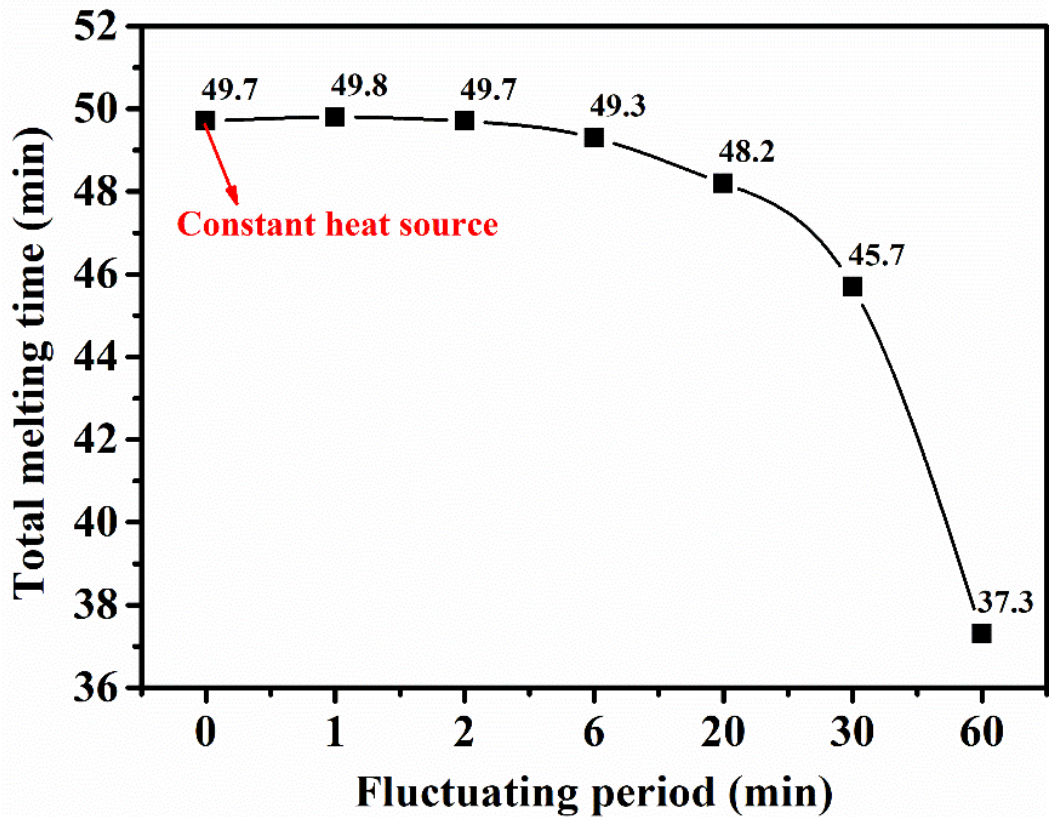

Fig. 6. The total melting time for fluctuating heat sources with different period.

The evolution of liquid volume fraction is related to the timewise heat flux transferred from HTF to PCM shown in **Fig. 7**. Taking the heat flux of the constant heat source as the baseline, it can be found that the heat flux of fluctuating heat sources fluctuates up and down the baseline with approximate symmetry. For a constant heat source, the heat flux gradually decreases with time because of the rise of the average PCM temperature. With regard to fluctuating heat sources, the heat flux presents wavelike

characteristics corresponding to the periodic variation of HTF temperature. For small-period fluctuating heat sources, the total heat flux varies in a large range with high frequency in every period, leading to the heat stored by PCM in a period very close to that of the constant heat source in the same time-lag, and this is the reason why there are minor differences in the evolution of liquid volume fraction between the fluctuating and constant heat sources. Nevertheless, that is not the case for large-period fluctuating heat sources.

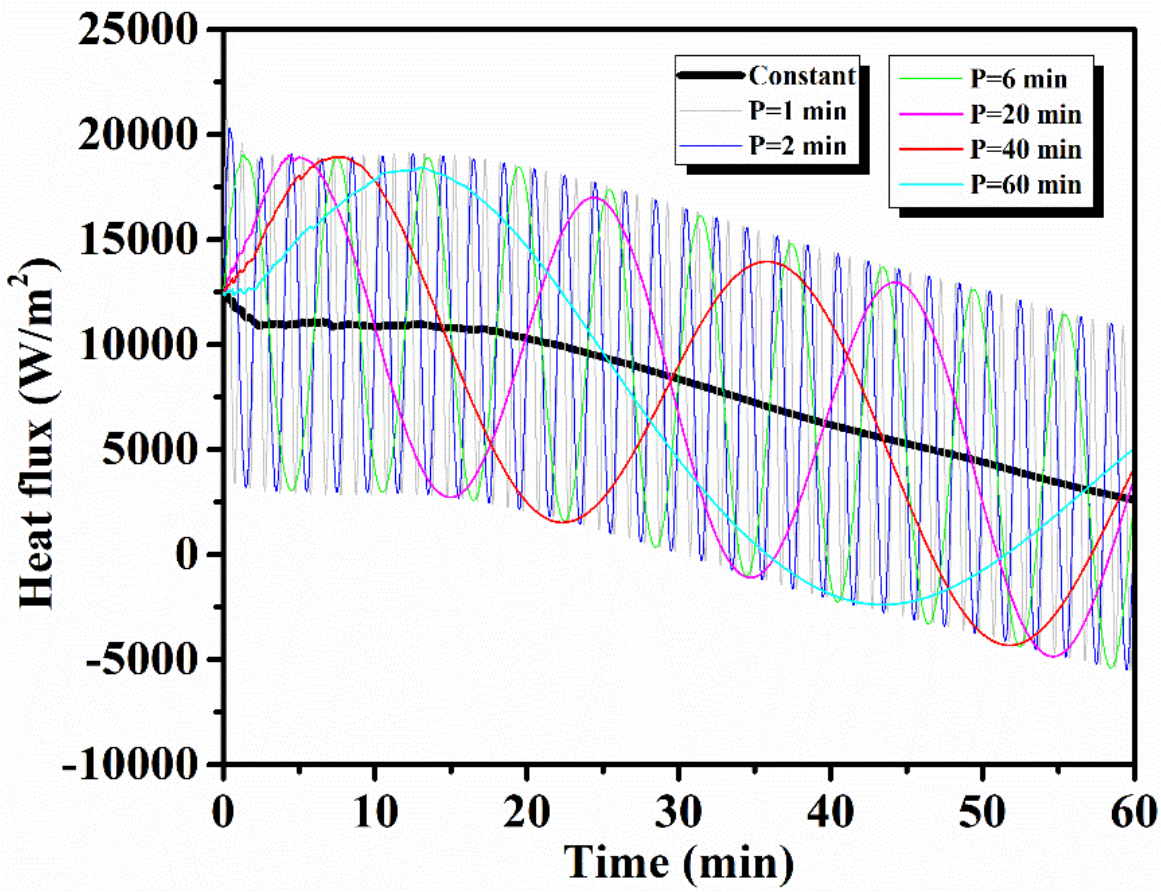

Fig. 7. The timewise heat flux for fluctuating heat sources with different period.

Fig. 8 demonstrates the heat absorbed by PCM in each unit time (1 minute). It can be seen that the heat absorbed by PCM in every minute for the case of P=1 min completely coincides with that of the constant heat source, resulting in their similar evolution of liquid volume fraction, i.e., almost the same melting

process. For the case of P=2 min and P=6 min, it can be shown that the total heat absorbed by PCM in a corresponding period has little difference with that of constant heat source in the same time-lag during the whole melting process, due to the symmetrical shape of total heat absorbed by PCM up and down the baseline in every corresponding time-lag. Particularly in the earlier stage of the melting process (t<10 min), an almost equal amount of heat transferred to the PCM cannot lead to significant natural convection in the liquid PCM due to the insignificant liquid volume fraction for both the constant heat source and fluctuating heat sources, and the heat transfer process is dominated by heat conduction, as a result, the fluctuating heat sources with small period make a little effect on the evolution of liquid volume fraction. However, for large-period fluctuating heat sources, the total heat absorbed by the PCM is significantly larger than that of the constant heat sources in the earlier stage of the melting process (t<10 min), which significantly enhances the heat transfer process of PCM and leads to large liquid volume fraction. In return, the natural convection existing in the liquid PCM improves the heat transfer rate between the HTF and PCM. As shown in **Fig. 5**, this reasoning explains the distinctly faster melting process of PCM for the large-period fluctuating heat sources compared with the constant heat source and small-period fluctuating heat sources in the early stage (t<20 min).

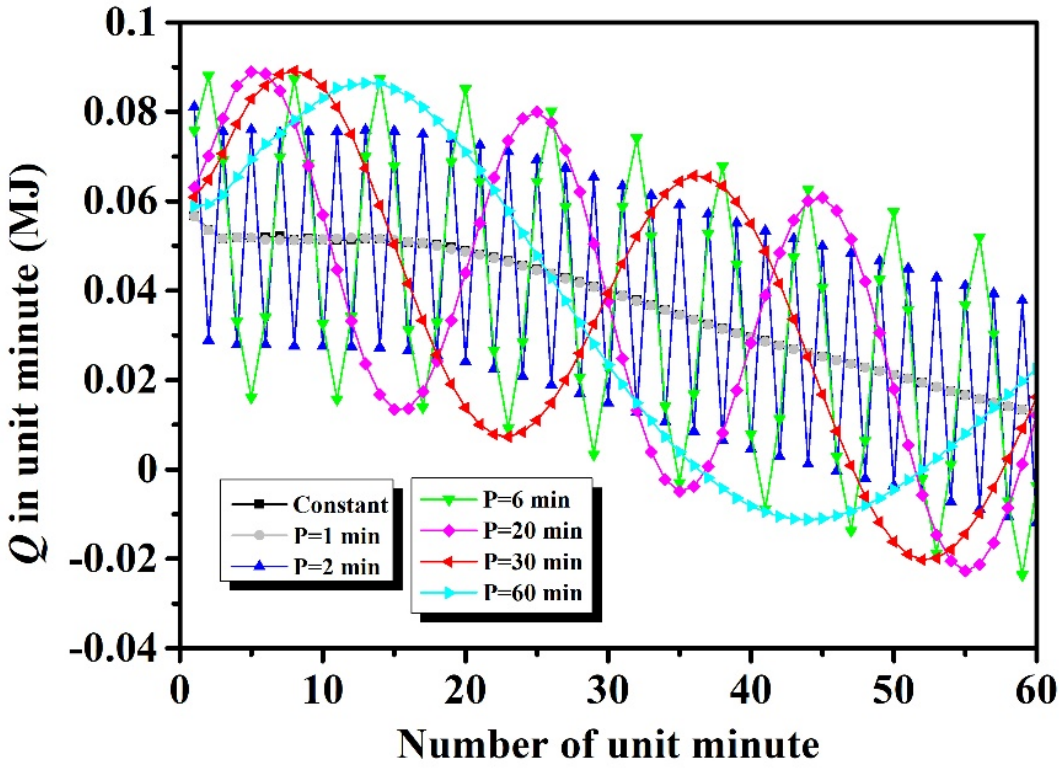

Fig. 8. The heat absorbed by PCM under different fluctuating heat sources in each unit time.

To further interpret the phenomenon, the temperature distribution and solid-liquid interface of PCM for different heat sources at different moments are presented in **Fig. 9**. The left semicircle is the temperature contour while the one on the right is the solid-liquid interface. Taking the results of the constant heat source as the comparison, the moments at t=300 s, t=550 s, t=1100 s and t=2000 s correspond to the moments of liquid volume fraction f=0.2, f=0.4, f=0.6 and f=0.8, respectively. It is apparent that the case of P=20 min shows the fastest melting process of PCM, while the case of P=30 min and P=60 min have minor effects to enhance the melting process at the moment of t=300 s, and the PCM average temperature of these cases shown in **Fig. 9** is significantly higher than that of constant heat source and small-period fluctuating heat sources. Results indicated the liquid volume fraction and the temperature contour of PCM has very little difference between the small-period fluctuating heat sources and constant heat sources at the moment of t=300 s. As the previous analysis of **Fig. 8** shows, the reason is related to

the total heat transferred to PCM in a time-lag. The total heat absorbed by PCM for small-period fluctuating heat sources (P= 1min, 2 min, 6 min) is almost the same as the constant heat source in the early stage of melting process, even for the whole melting process, bringing about a limited difference in the evolution of liquid volume fraction and contour temperature. However, the large-period fluctuating heat sources can transfer much more heat to the PCM during the earlier stage (t<10 min), even the early stage (t<20 min) of the melting process, therefore, the liquid volume fraction rises rapidly and natural convection occurs in the liquid PCM, in turn improving the melting rate. For example, in the first 5 minutes of the melting process, the case of P=20 min transfers the most heat to the PCM, leading to the highest average temperature and liquid volume fraction of PCM among all the heat sources shown in **Fig. 9**.

At the moment of t=550 s, 1100 s and 2000 s, it can be shown that the difference in the solid-liquid interface and temperature distribution of PCM is still unapparent between the small-period fluctuating heat sources and constant heat source, owing to the similar amount of heat transferred to PCM during every corresponding time-lag. That can explain the narrow margin in the evolution of liquid volume fraction for the small-period fluctuating heat sources and constant heat source. However, for the large-period fluctuating heat sources, various degrees of enhancement effects are observed corresponding to different periods compared with the constant heat source. The larger the fluctuating period, the more substantial enhancement effects can be observed. That is relevant to the scale of the period. For the case of P=20 min and P=30 min, their timewise heat flux in the latter half period is quite small compared to that of the former half period in a whole period, which is also smaller than that of the constant heat source in the corresponding time-lag, leading to lower increasing rate of average temperature and liquid

volume fraction, as well as diminishing the enhancement effects in the subsequent melting process. For the case of P=60 min, the liquid volume fraction exceeds 90% in the first half period, therefore, its large enhancement effects in the melting process can be maintained in the later period. From the whole melting process for all the cases, it is determined that the difference of average temperature keeps decreasing between the small-period fluctuating heat sources and the large-period cases with the evolution of the melting process. That is because the heat is mainly stored by the sensible heat instead of latent heat in the later melting process for the large-period fluctuating heat source. Therefore the temperature difference inside the liquid PCM declines quickly, making the average temperature very similar with each other under different cases, as well as the liquid volume fraction of small-period fluctuating heat source is very close to that of the large-period fluctuating heat source. The results demonstrated the importance of heat transfer enhancement for the late melting process of LTES under fluctuating heat source.

In addition to the melting rate, the energy storage capacity is another crucial indicator used to evaluate the performance of LTES. From **Fig. 10** it can be seen that the total energy stored by PCM of all the fluctuating heat sources are less than that of the constant heat source. Additionally, the total heat stored by PCM decreases with the increase of the fluctuating period. It is noticed that the total stored heat by PCM of small-period fluctuating heat sources is almost equal to that of the constant heat source, but the difference enlarges significantly when the fluctuating period increases to P=20 min. For the case of P=60 min, the largest difference in heat stored by PCM leads to approximately 9.5% smaller energy storage capacity in contrast to the constant heat source.

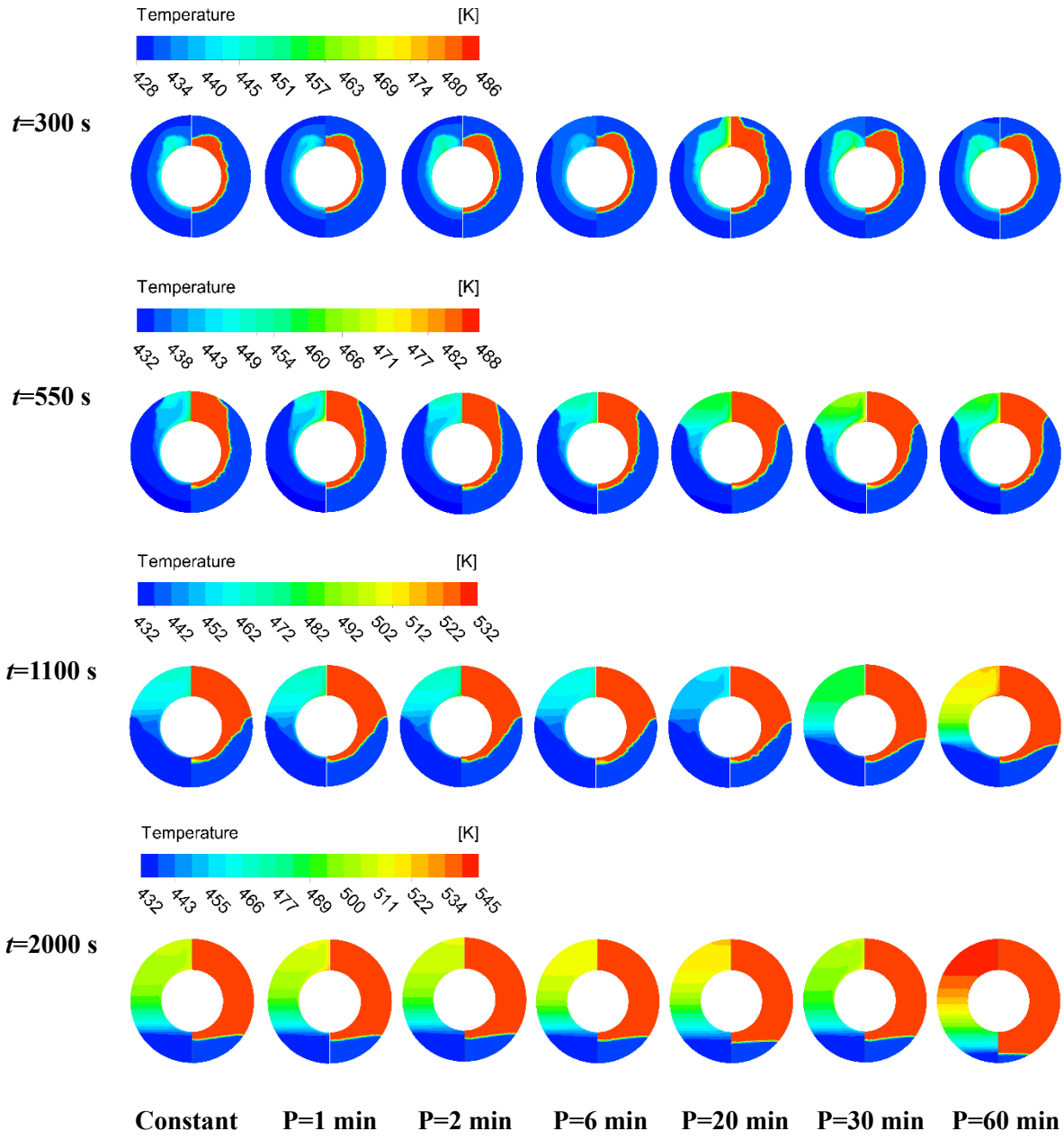

Fig. 9. The temperature contour and the liquid-solid interface at different moments. Left semicircle: temperature contour; Right semicircle: liquid-solid interface.

The reason for this is related to the temperature distribution during the melting process shown in **Fig. 9**. As previously explained, the small-period fluctuating (P= 1 min, 2 min, 6 min) heat sources lead to similar evolution of liquid volume fraction and temperature field to the constant heat source, i.e., the similar temperature difference during the heat transfer process between the HTF and PCM. For large-

period fluctuating heat sources (P= 20 min, 30 min, 60 min), the enhancement effects of melting process are larger with the increase of period compared to the constant heat source, as a consequence, the stage of sensible heat storage is faster to be achieved, for example, the higher average temperature and smaller temperature difference during the heat transfer process between the HTF and PCM.

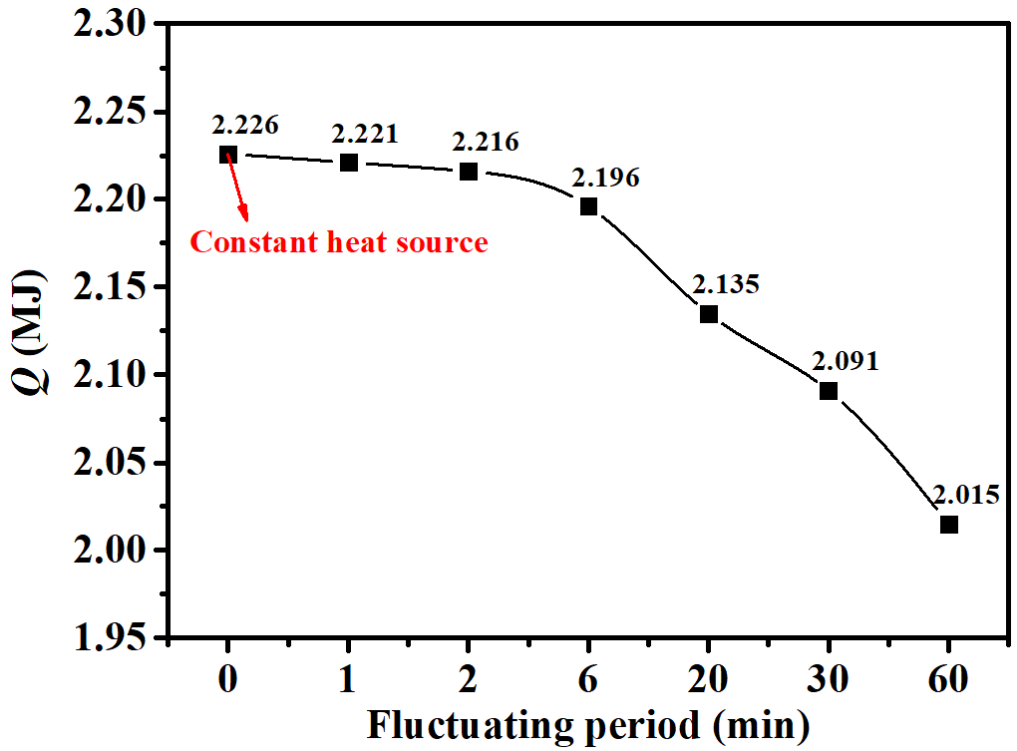

Fig. 10. The total energy stored by PCM under fluctuating heat sources with different period.

4.2 Effects of fluctuating amplitude

According to the previous analysis, only the larger fluctuating periods leads to significant enhancement effects on the heat transfer performance of LTES. In this section, the effects of different amplitudes of fluctuating heat sources with their fluctuating periods fixed at P=60 min are investigated in detail. Comparing with the constant heat source, it is apparent in **Fig. 11** that all the fluctuating heat sources can accelerate the evolution of PCM liquid volume fraction and the enhancement effect keeps

improving when the fluctuating amplitude increases from 50 K to 150 K. For each fluctuating heat source, the enhancement effect is not evident at first and then continues to augment until the completion of the melting process, in contrast to the constant heat source. The total melting for different heat sources is depicted in **Fig. 12**. Compared to the total melting time of the constant heat source (49.7 min), the total melting time for fluctuating heat sources dramatically decreases with the enlargement of fluctuating amplitude. It is 44.2 min for the case of A=50 K while the value is 32.3 min for the case of A=150 K, and the total melting time is shortened by 11.1% and 35.0%, respectively.

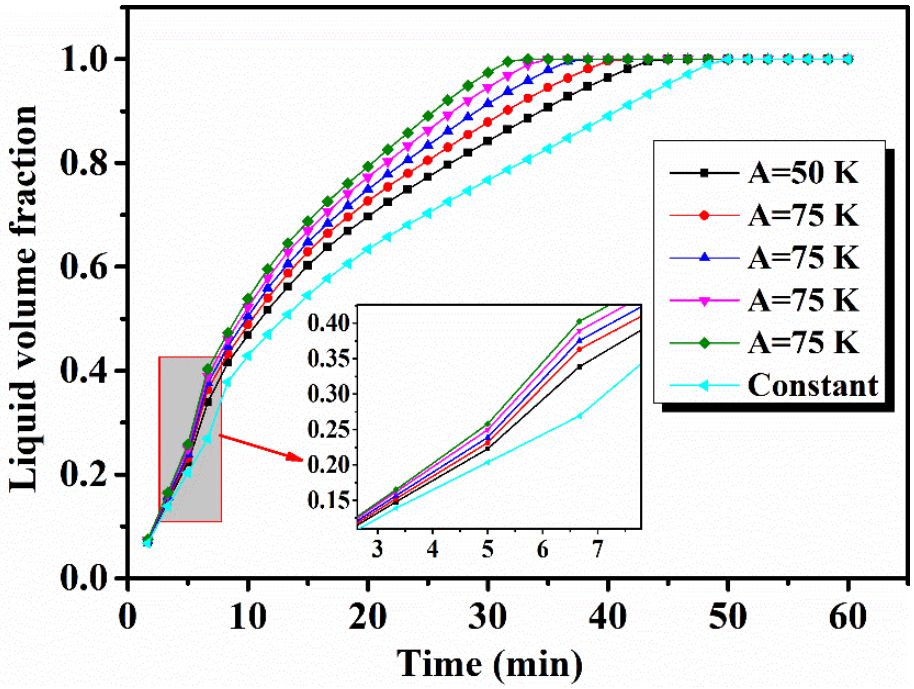

Fig. 11. The evolution of liquid volume fraction with melting time under different heat sources.

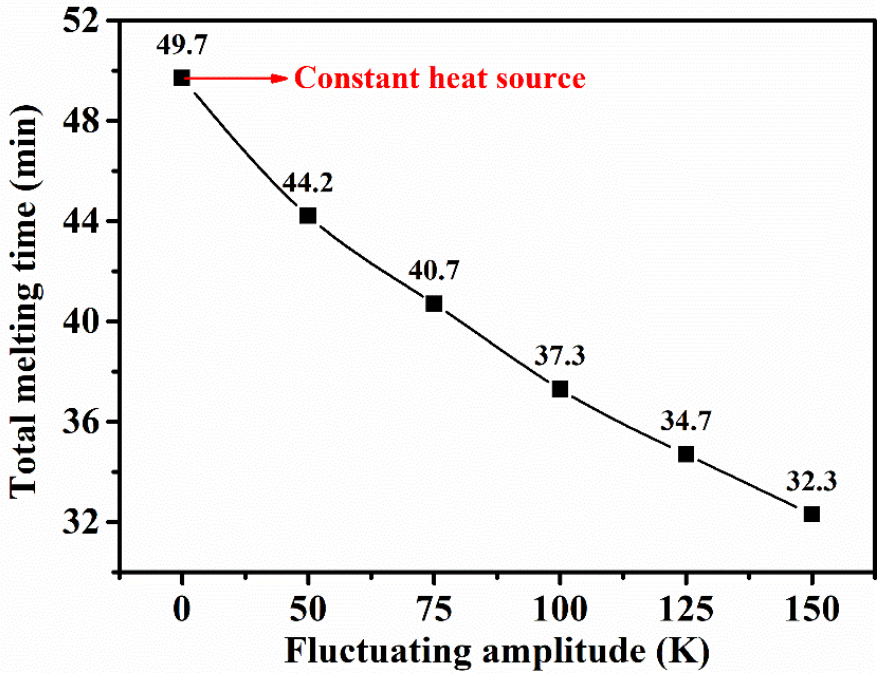

Fig. 12. The total melting time for fluctuating heat sources under different fluctuating amplitude

Based on the previous analysis, it can be understood that the effects of fluctuating amplitude are different from that of the fluctuating period. For the impacts of the fluctuating period, the large-period heat sources have significant enhancement effects on the heat transfer performance of LTES while the small-period fluctuating heat sources have almost no effect, as previously explained. But all the heat sources with different amplitudes have evident enhancement effects on the heat transfer performance of LTES to a different extent. This is related to the melting process of LTES determined by the heat flux between the HTF and PCM. **Fig. 13** shows the comparison of timewise heat flux for a constant heat source and fluctuating heat sources with different fluctuating amplitude. For a constant heat source, the heat flux gradually decreases during the whole melting process because the increase of the PCM temperature leads to a continuously small temperature difference between the HTF and PCM. For each case of fluctuating heat source, the heat flux presents the wavelike characteristic just like the temperature variation of HTF. The timewise heat flux first increases due to the increase of HTF

temperature, then it decreases rapidly to the bottom because of the decline of HTF temperature and increase of PCM temperature, and later it begins to increase again from the bottom owing to the rise of the HTF temperature.

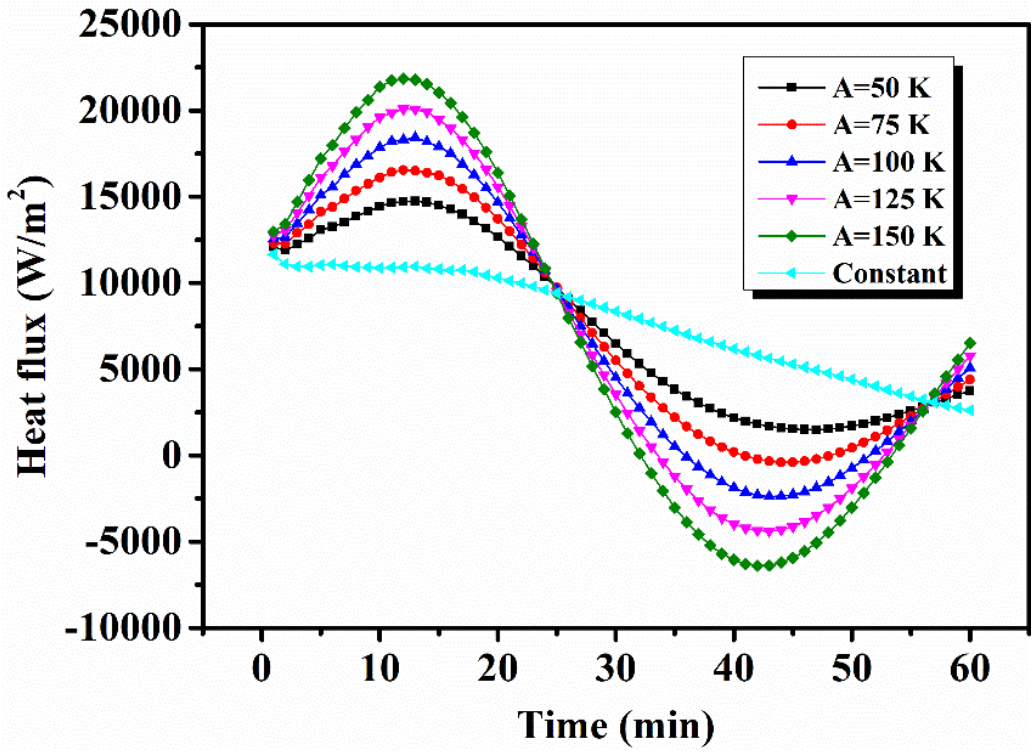

Fig. 13. The timewise heat flux for fluctuating heat sources with different fluctuating amplitude.

Taking the heat flux of constant heat source as the baseline, it can be shown that the heat flux of fluctuating heat sources is relatively large before the moment of the first-half period (about the moment of t=25 min), which explains why the fluctuating heat sources with different fluctuating amplitudes accelerate the melting process of LTES, as shown in **Fig. 11**. With the increasing liquid volume fraction, the natural convection occurring in the liquid PCM enhances and it strengthens the heat transfer process between the PCM and HTF. Although the heat flux of fluctuating heat sources is smaller than that of the constant heat source during the second half period of the melting process, the natural convection can enhance the heat transfer process inside the PCM, which weakens the adverse effects of the decline

of heat flux on the heat transfer process.

To further illustrate the phenomenon, the temperature distribution (left semicircle) and solid-liquid interface (right semicircle) of PCM for different heat sources at different moments are presented in **Fig. 14**. Similar to the analysis of the effects of fluctuating periods, the results of constant heat source are taken as the comparison, and the moments at t=300 s, t=550 s, t=1100 s and t=2000 s correspond to the moments of liquid volume fraction f=0.2, f=0.4, f=0.6 and f=0.8 for a constant heat source, respectively. At the moment of t=300 s, the enhancement effects on the temperature contour and liquid volume fraction are relatively insignificant compared to the constant heat source, since the difference in the heat flux between the constant and fluctuating heat source is small and the total amount of heat transferred to the PCM is small in this short time-lag. When the melting process reaches the moment of t=550 s, the liquid volume fraction and the average temperature of PCM for a constant heat source is significantly lower than that of fluctuating heat sources. Furthermore, the fluctuating heat source with larger fluctuating amplitude appears to result in higher liquid volume fraction and average PCM temperature in contrast to that of the small-amplitude fluctuating heat sources. That is because the difference in the heat flux among all the fluctuating heat sources keeps enlarging with the increase of the fluctuating amplitude. The difference in the heat flux continues to increase before it attains the top and then it maintains a high level before the moment of t=20 min as shown in **Fig. 13**, which can explain why the fluctuating heat sources bring about increasing average PCM temperature and liquid volume fraction compared to the constant heat sources during the early stage (t<20 min) of the melting process, as well as the increasing difference in average PCM temperature and liquid volume fraction among the fluctuating heat sources. For example, at the moment of t=1100 s, the maximum temperature differences

between the constant heat source and the fluctuating case of A=50 K and A=150 K are 26 K and 89 K, respectively, while they are only 12 K and 31 K at the moment of *t*=550 s.

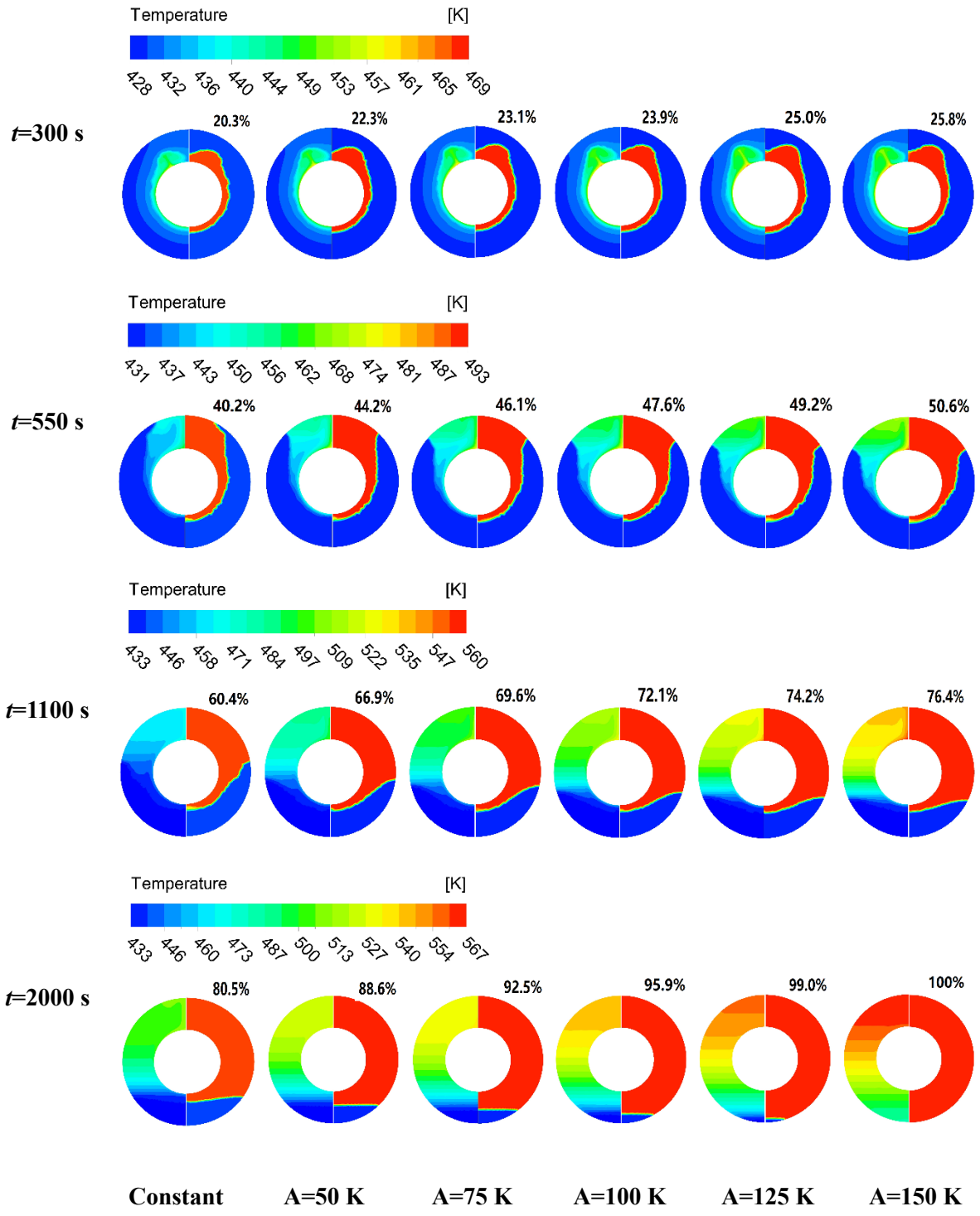

Fig. 14. The temperature contour and the liquid-solid interface at different moments. Left

semicircle: temperature contour; Right semicircle: liquid-solid interface.

With the continuous evolution of the melting process, the heat flux for a constant heat source is larger than that of all the fluctuating heat sources, and among all the fluctuating heat sources smaller fluctuating amplitude leads to a higher heat flux due to the sinusoidal variation of HTF temperature as shown in **Fig. 13**. Despite the opposite variation trend of heat flux for constant and fluctuating heat sources, most of the PCM for each case has melted at this time and the thermal conduction is dominant instead of natural convection during the later stage of melting process. And the main energy storage mode is sensible energy storage of liquid PCM instead of latent heat storage of solid PCM, which means the residual solid PCM at the bottom melts very slowly due to the low thermal conductivity of PCM extending the total melting time of the melting process. For example, at the moment of t=2000 in **Fig. 14**, it can be observed that the difference in average PCM temperature and liquid volume fraction among the constant heat source and fluctuating heat sources decreases with less extent compared to the previous moments, but the case of A=150 almost completes the melting process (f=1) while the constant case only attains f=0.8.

As for the energy storage capacity of LTES under different heat sources depicted in **Fig. 15**, it can be observed that LTES heated by the constant heat source obtains the maximum energy storage capacity. The energy storage capacity of fluctuating heat sources decreases with the rise of the fluctuating amplitude. The energy storage capacity for A=50 K and A=150 K is 4.5% and 28.5% smaller than that of constant heat source, respectively. The reason is related to the temperature distribution of PCM during the melting process shown in **Fig. 14**. In the first half period, the PCM temperature, under fluctuating heat sources, increases rapidly due to the higher heat flux compared to the constant heat source, leading

to the decline of the temperature difference between the HTF and PCM. In the second half period, the PCM temperature, under fluctuating heat sources, continues to increase but the HTF temperature is under the average temperature of HTF. Therefore, the PCM average temperature under fluctuating heat source is higher than that of constant heat source at any moments during the melting process, and the average PCM temperature improves with the rise of fluctuating heat source. However, the average temperature of HTF is fixed for all the heat sources in a period, that is, the lower temperature difference between the PCM and constant heat source achieves the maximum energy storage capacity, while the energy storage capacity decreases with the improvement of fluctuating amplitude for fluctuating heat sources.

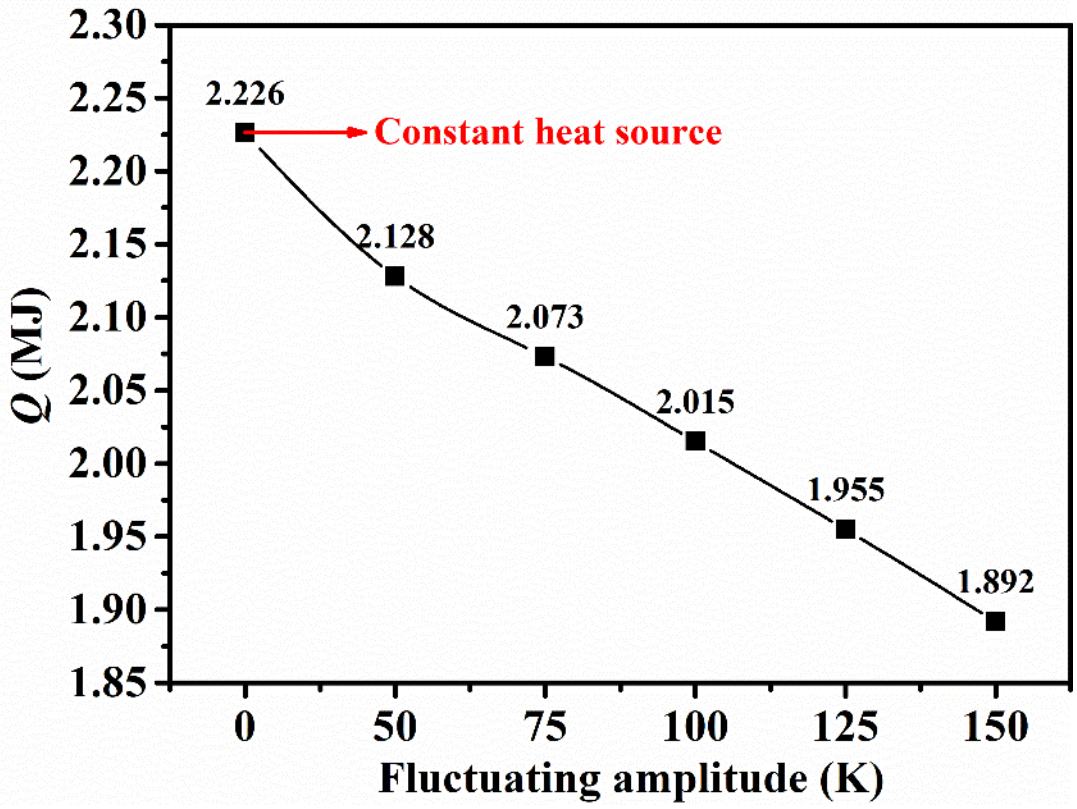

Fig. 15. The total energy stored by PCM under fluctuating heat sources with different amplitude.

4.3 Analysis of Stefan number

To evaluate the effects of different inlet temperatures of HTF on the melting process of LTES, the dimensionless Stefan number is used to describe the relationship of HTF temperature and melting temperature, and it is defined in the following formulation:

$$Ste = \frac{c_{p,p}\left(T_{av} - T_m\right)}{L} \tag{16}$$

According to the analysis of fluctuating period in Section 4.1, the fluctuating heat sources with small periods result in a similar melting process to the constant heat source. Therefore, the effects of the fluctuating period under different Stefan numbers are investigated in this section. **Fig. 16** shows the evolution of liquid volume fraction of LTES under fluctuating heat sources with different fluctuating period and Stefan number. For a certain *Ste* number, the fluctuating heat source with a larger period leads to faster melting process just as previously analysed. With the increase of *Ste* number, it can be observed that the evolution of liquid volume fraction of P=2 min is closer to that of P=20 min and P=60 min, which indicates that larger *Ste* number can motivate the enhancement effects of fluctuating heat source with P=2 min to a certain extent. That is because the larger *Ste* number means higher inlet temperature of HTF, resulting in larger heat flux and therefore larger liquid volume fraction in a corresponding period. Then the natural convection occurs earlier to enhance the heat transfer process in return and diminish the difference in melting rate between the case of P=2 min and cases with a larger period of P=20 min and 60 min.

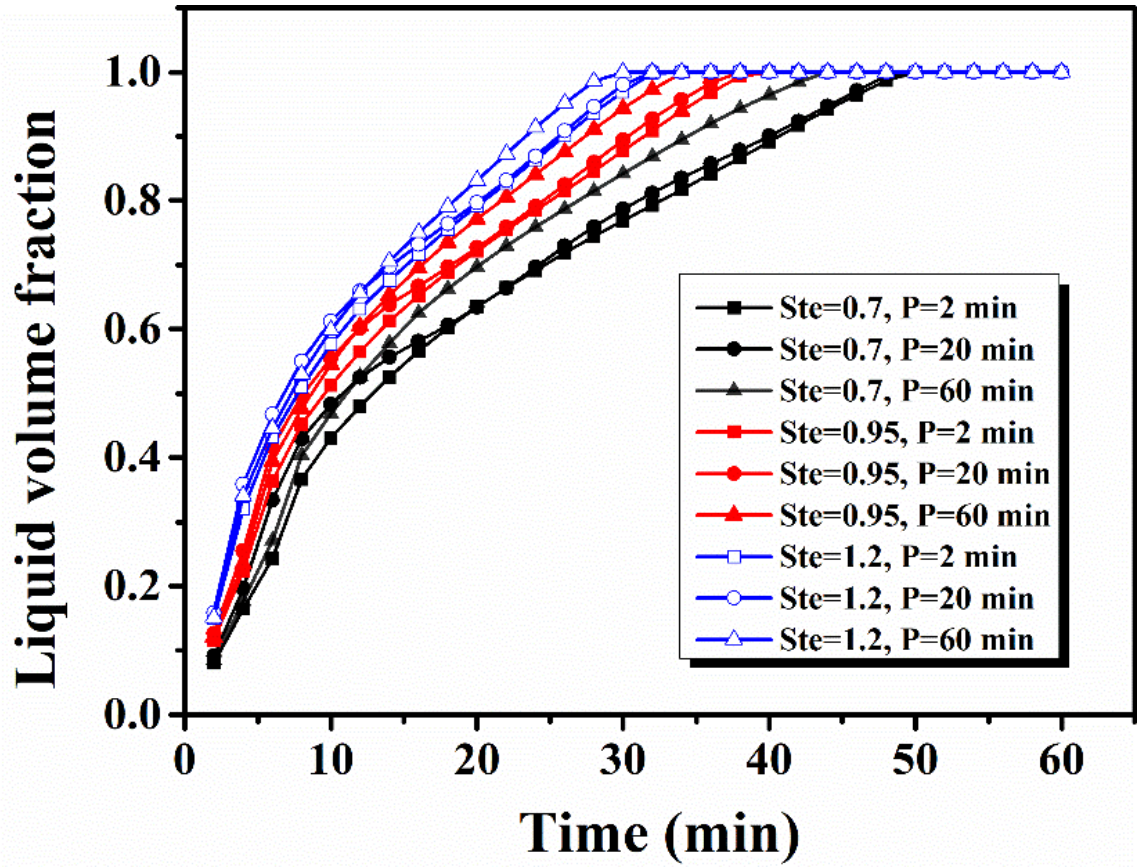

Fig. 16. The evolution of liquid volume fraction with melting time under different Stefan Numbers.

Fig. 17 indicates the corresponding total melting time for fluctuating heat sources under different *Ste* numbers. For any fixed period, the total melting declines in an increasing rate with the increase of *Ste* number because of the rise of average inlet temperature of HTF. However, the declining trend of total melting time is more rapid for a smaller-period fluctuating heat source. Additionally, the difference in total melting between P=2 min and P=60 min decreases with the increase of *Ste* number. For example, the difference is 17.4 min between the P=2 min and P=60 min when the *Ste* number is equal to 0.7, whereas it is 17.1 min and 15 min for the case of *Ste*=0.95 and *Ste*=1.2, respectively. The total energy stored by PCM for each case is shown in **Fig. 18**. For any fixed *Ste* number, the case of P=2 min stores the maximum amount of heat during the whole melting process while the case of P=60 min ranks last. For any fixed period, the energy storage capacity rises with the increase of *Ste* number. It also can be

observed that the difference in energy storage capacity among these three cases enlarges with the increase of *Ste* number, which indicates the fluctuating heat source with smaller period can bring about greater energy storage capacity for LTES under the condition of larger *Ste* number.

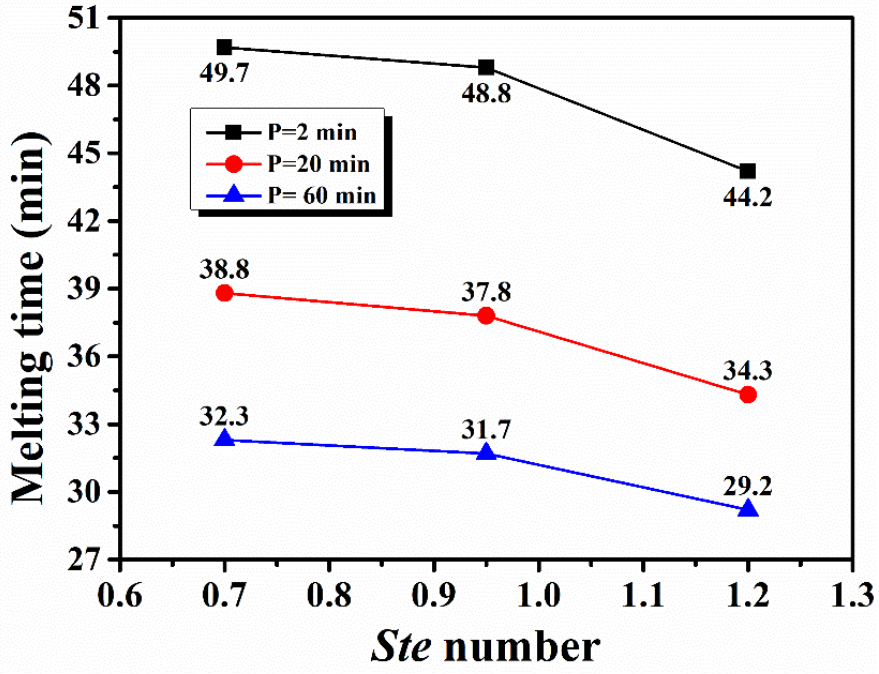

Fig. 17. The total melting time for fluctuating heat sources under different Stefan Numbers.

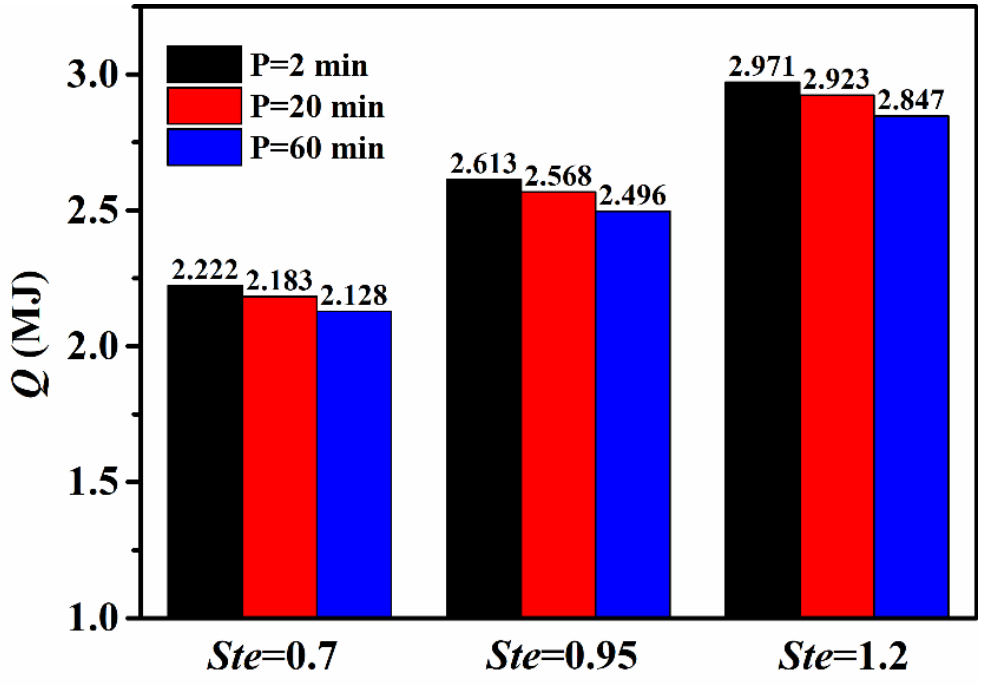

Fig. 18. The total energy stored by PCM under fluctuating heat sources with different Stefan

Numbers

5. Conclusions and prospects

In this study, the heat transfer performance of a shell-and-tube LTES heated by fluctuating heat sources is analysed to overcome the barriers in waste heat recovery caused by fluctuating heat sources. The effects of factors including period, amplitude and Stefan number of fluctuating heat source investigated in detail. Some conclusions are drawn, as follows:

(1) Fluctuating heat sources with large period can significantly enhance the melting rate and shorten the total melting time, as well as lead to a smaller energy storage capacity of LTES compared to the constant heat source. Whilst the fluctuating heat sources with small period has almost no effect on both the total melting time and energy storage capacity of LTES. For example, the total melting time and energy storage capacity for P=60 min are reduced by 24.5% and 9.5% in contrast to that of constant heat source, but they are almost the same for the case of P=1 min, 2 min and 6 min. The results indicate that the high-frequency fluctuation of fluctuating heat sources can be ignored when designing the LTES for heat recovery applications.

(2) Fluctuating heat sources with different amplitudes can substantially reduce the melting time and energy storage capacity of LTES in contrast to the constant heat source. Furthermore, both the total melting time and energy storage capacity decline at a decreasing rate with the increase of fluctuating amplitude. In detail, compared with a constant heat source, the case of A=50 K and A=150 K respectively reduce the total melting time by 11.1%, 35.0% and energy storage capacity by 4.4%, 15.0%

(3) Stefan number analysis method is used to evaluate the effects of different inlet temperature of HTF on the melting process of LTES. The results illustrate that the fluctuating heat source with a larger period leads to faster melting process under a fixed Stefan number. But the total melting time of small-period fluctuating heat source gets closer to that of a larger-period fluctuating heat source with the improvement of Stefan number.

(4) Fluctuating heat sources improve the melting rate of PCM, and therefore accelerate the melting process, but they lead to smaller energy storage capacity due to the inferior performance of temperature uniformity. T hat is, there is a discrepancy between the melting rate and energy storage capacity. In the future designs of LTES for fluctuating heat source, heat transfer enhancement technologies such as heat pipes should be explored to improve the temperature uniformity.

Although the effects of period and amplitude for fluctuating heat source on the heat transfer process of LTES is separately analysed in this study, the coupling effects of period and amplitude should be further investigated. In detail, mapping studies to illustrate the relationship of melting time and energy storage capacity with the period and amplitude of fluctuating heat source should be obtained. Additionally, other important factors including the flowrate of fluctuating heat source, as well as the thermophysical properties of PCM, especially the thermal conductivity, need to be carefully evaluated to reveal the comprehensive heat transfer mechanism of LTES under fluctuating heat source.

Acknowledgements

This research project was funded by the National Natural Science Foundation of China (grant numbers No. 51976176 and No. 51806189). Support from the China Science Foundation (grant numbers 2018M640556 and2019T120514) and Zhejiang Province Science Foundation (grant number ZJ20180099) are also gratefully acknowledged. The authors would also like to thank the Royal

Academy of Engineering through the Transforming Systems through Partnerships programme (Grant Number TSPC1098)and Newton Fund Innovation Partnership (Grant number 201703780098).

Reference

[1] Li X, Tian H, Shu G, Hu C, Sun R, Li L. Effects of external perturbations on dynamic performance of carbon dioxide transcritical power cycles for truck engine waste heat recovery. Energy. 2018;163:920-31.

[2] Song J, Li X-s, Ren X-d, Gu C-w. Performance analysis and parametric optimization of supercritical carbon dioxide (S-CO2) cycle with bottoming Organic Rankine Cycle (ORC). Energy. 2018;143:406-16.

[3] Dal Magro F, Jimenez-Arreola M, Romagnoli A. Improving energy recovery efficiency by retrofitting a PCM-based technology to an ORC system operating under thermal power fluctuations. Applied Energy. 2017;208:972-85.

[4] Li X, Tian H, Shu G, Zhao M, Markides CN, Hu C. Potential of carbon dioxide transcritical power cycle waste-heat recovery systems for heavy-duty truck engines. Applied Energy. 2019;250:1581-99.

[5] Nardin G, Meneghetti A, Dal Magro F, Benedetti N. PCM-based energy recovery from electric arc furnaces. Applied Energy. 2014;136:947-55.

[6] Dal Magro F, Meneghetti A, Nardin G, Savino S. Enhancing energy recovery in the steel industry: Matching continuous charge with off-gas variability smoothing. Energy Conversion and Management. 2015;104:78-89.

[7] Liu G, Liu J, E J, Li Y, Zhang Z, Chen J, et al. Effects of different sizes and dispatch strategies of thermal energy storage on solar energy usage ability of solar thermal power plant. Applied Thermal Engineering. 2019;156:14-22.

[8] Jafari Mosleh H, Ahmadi R. Linear parabolic trough solar power plant assisted with latent thermal energy storage system: A dynamic simulation. Applied Thermal Engineering. 2019;161:114204.

[9] Li S, Ma H, Li W. Dynamic performance analysis of solar organic Rankine cycle with thermal energy storage. Applied Thermal Engineering. 2018;129:155-64.

[10] Freeman J, Guarracino I, Kalogirou SA, Markides CN. A small-scale solar organic Rankine cycle combined heat and power system with integrated thermal energy storage. Applied Thermal Engineering. 2017;127:1543-54.

[11] Dal Magro F, Savino S, Meneghetti A, Nardin G. Coupling waste heat extraction by phase change materials with superheated steam generation in the steel industry. Energy. 2017;137:1107-18.

[12] Yu X, Li Z, Lu Y, Huang R, Roskilly AP. Investigation of organic Rankine cycle integrated with double latent thermal energy storage for engine waste heat recovery. Energy. 2019;170:1098-112.

[13] Xu ZY, Wang RZ, Yang C. Perspectives for low-temperature waste heat recovery. Energy. 2019;176:1037-43.

[14] Guo C, Zhang W. Numerical simulation and parametric study on new type of high temperature latent heat thermal energy storage system. Energy Conversion and Management. 2008;49(5):919-27.

[15] Wang W-W, Zhang K, Wang L-B, He Y-L. Numerical study of the heat charging and discharging characteristics of a shell-and-tube phase change heat storage unit. Applied Thermal Engineering. 2013;58(1):542-53.

[16] Tao YB, Carey VP. Effects of PCM thermophysical properties on thermal storage performance of a shell-and-tube latent heat storage unit. Applied Energy. 2016;179:203-10.

[17] Agyenim F, Eames P, Smyth M. A comparison of heat transfer enhancement in a medium temperature thermal energy storage heat exchanger using fins. Solar Energy. 2009;83(9):1509-20.

[18] Wang P, Yao H, Lan Z, Peng Z, Huang Y, Ding Y. Numerical investigation of PCM melting process in sleeve tube with internal fins. Energy Conversion and Management. 2016;110:428-35.

[19] Ebrahimi A, Hosseini MJ, Ranjbar AA, Rahimi M, Bahrampoury R. Melting process investigation of phase change materials in a shell and tube heat exchanger enhanced with heat pipe. Renewable Energy. 2019;138:378-94.

[20] Das N, Takata Y, Kohno M, Harish S. Effect of carbon nano inclusion dimensionality on the melting of phase change nanocomposites in vertical shell-tube thermal energy storage unit. International Journal of Heat and Mass Transfer. 2017;113:423-31.

[21] Yang X, Yu J, Guo Z, Jin L, He Y-L. Role of porous metal foam on the heat transfer enhancement for a thermal energy storage tube. Applied Energy. 2019;239:142-56.

[22] Tao YB, He YL, Liu YK, Tao WQ. Performance optimization of two-stage latent heat storage unit based on entransy theory. International Journal of Heat and Mass Transfer. 2014;77:695-703.

[23] Fang Y, Niu J, Deng S. An analytical technique for the optimal designs of tube-in-tank thermal energy storage systems using PCM. International Journal of Heat and Mass Transfer. 2019;128:849-59.

[24] Deng S, Nie C, Jiang H, Ye W-B. Evaluation and optimization of thermal performance for a finned double tube latent heat thermal energy storage. International Journal of Heat and Mass Transfer. 2019;130:532-44.

[25] Tao YB, He YL. Numerical study on thermal energy storage performance of phase change material under non-steady-state inlet boundary. Applied Energy. 2011;88(11):4172-9.

[26] Elbahjaoui R, El Qarnia H. Numerical Study of a Shell-and-Tube Latent Thermal Energy Storage Unit Heated by Laminar Pulsed Fluid Flow. Heat Transfer Engineering. 2017;38(17):1466-80.

[27] Xu HJ, Zhao CY. Thermal performance of cascaded thermal storage with phase-change materials (PCMs). Part II: Unsteady cases. International Journal of Heat and Mass Transfer. 2017;106:945-57.

[28] Huo Y, Zong J, Rao Z. The investigations on the heat transfer in thermal energy storage with time-

dependent heat flux for power plants. Energy. 2019;175:1209-21.

[29] Jiménez-Arreola M, Pili R, Dal Magro F, Wieland C, Rajoo S, Romagnoli A. Thermal power fluctuations in waste heat to power systems: An overview on the challenges and current solutions. Applied Thermal Engineering. 2018;134:576-84.

[30] Pereira da Cunha J, Eames P. Thermal energy storage for low and medium temperature applications using phase change materials – A review. Applied Energy. 2016;177:227-38.

[31] Tao YB, He YL. Effects of natural convection on latent heat storage performance of salt in a horizontal concentric tube. Applied Energy. 2015;143:38-46.

[32] Al-Abidi AA, Mat S, Sopian K, Sulaiman MY, Mohammad AT. Numerical study of PCM solidification in a triplex tube heat exchanger with internal and external fins. International Journal of Heat and Mass Transfer. 2013;61:684-95.

[33] Deng S, Nie C, Wei G, Ye W-B. Improving the melting performance of a horizontal shell-tube latent-heat thermal energy storage unit using local enhanced finned tube. Energy and Buildings. 2019;183:161-73.

[34] Lacroix M. Numerical simulation of a shell-and-tube latent heat thermal energy storage unit. Solar Energy. 1993;50(4):11.